The substitutions L50F, E166A and L167F in SARS-CoV-2 3CLpro are selected by a protease inhibitor *in vitro* and confer resistance to nirmatrelvir

Dirk Jochmans[$1], Cheng Liu[2], Kim Donckers[1], Antitsa Stoycheva[2], Sandro Boland[3], Sarah K Stevens[2], Chloe De Vita[2], Bert Vanmechelen[4], Piet Maes[4], Bettina Trüeb[5], Nadine Ebert[5], Volker Thiel[5], Steven De Jonghe[1], Laura Vangeel[1], Dorothée Bardiot[3], Andreas Jekle[2], Lawrence M Blatt[2], Leonid Beigelman[2], Julian A Symons[2], Pierre Raboisson[6], Patrick Chaltin[7], Arnaud Marchand[3], Johan Neyts[$8], Jerome Deval[*2], Koen Vandyck[*6]

[*] Shared Last authorship
[$] Corresponding author: dirk.jochmans@kuleuven.be and johan.neyts@kuleuven.be

[1] KU Leuven, Department of Microbiology, Immunology & Transplantation, Rega Institute, Laboratory of Virology & Chemotherapy, Herestraat 49, 3000 Leuven, Belgium.
[2] Aligos Therapeutics, Inc., 1 Corporate Dr., 2nd Floor, South San Francisco, CA, USA.
[3] CISTIM Leuven vzw, Gaston Geenslaan 2, 3001 Leuven, Belgium.
[4] KU Leuven, Department of Microbiology, Immunology & Transplantation, Rega Institute, Laboratory of Clinical & Epidemiological Virology, Herestraat 49, Leuven, 3000, Belgium.
[5] Institute of Virology and Immunology, University of Bern, 3012, Bern, Switzerland; Department of Infectious Diseases and Pathobiology, Vetsuisse Faculty, University of Bern, Bern, Switzerland.
[6] Aligos Belgium BV, Gaston Geenslaan 1, 3001 Leuven, Belgium.
[7] Centre for Drug Design and Discovery (CD3), KU Leuven, Gaston Geenslaan 2, 3001 Leuven, Belgium; CISTIM Leuven vzw, Gaston Geenslaan 2, 3001 Leuven, Belgium.
[8] KU Leuven, Department of Microbiology, Immunology & Transplantation, Rega Institute, Laboratory of Virology & Chemotherapy, Herestraat 49, 3000 Leuven, Belgium and Global Virus Network (GVN)

Abstract

The SARS-CoV-2 main protease (3CLpro) has an indispensable role in the viral life cycle and is a therapeutic target for the treatment of COVID-19. The potential of 3CLpro-inhibitors to select for drug-resistant variants needs to be established. Therefore, SARS-CoV-2 was passaged *in vitro* in the presence of increasing concentrations of ALG-097161, a probe compound designed in the context of a 3CLpro drug discovery program. We identified a combination of amino acid substitutions in 3CLpro (L50F E166A L167F) that is associated with > 20x increase in EC_{50} values for ALG-097161, nirmatrelvir (PF-07321332) and PF-00835231. While two of the single substitutions (E166A and L167F) provide low-level resistance to the inhibitors in a biochemical assay, the triple mutant results in the highest levels of resistance (6x to 72x). All substitutions are associated with a significant loss of enzymatic 3CLpro activity, suggesting a reduction in viral fitness. Structural biology analysis indicates that the different substitutions reduce the number of inhibitor/enzyme interactions while the binding of the substrate is maintained. These observations will be important for the interpretation of resistance development to 3CLpro inhibitors in the clinical setting.

Abstract Importance

Paxlovid is the first oral antiviral approved for treatment of SARS-CoV-2 infection. Antiviral treatments are often associated with the development of drug resistant viruses. In order to guide the use of novel antivirals it is essential to understand the risk of resistance development and to characterize the associated changes in the viral genes and proteins. In this work, we describe for the first time a pathway that allows SARS-CoV-2 to develop resistance against Paxlovid *in vitro*. The characteristics of *in vitro* antiviral resistance development may be predictive for the clinical situation. Therefore, our work will be important for the management of COVID-19 with Paxlovid and next generation SARS-CoV-2 3CLpro inhibitors.

Introduction

There is an urgent need for potent and safe antiviral drugs for the treatment and prophylaxis of SARS-CoV-2 infections. Highly efficacious and safe viral protease inhibitors have contributed significantly to the effective treatment of infections with HIV and HCV. Coronaviruses have two proteases, the main protease 3CLpro (or Mpro) and the papain-like protease. 3CLpro is a cysteine protease that cleaves the two polyproteins (pp1a and pp1ab) of SARS-CoV-2 at eleven different sites, resulting in various non-structural proteins, which are key for viral replication [1]. The substrate of 3CLpro presents a distinct glutamine at the P1 site (Leu-Gln/Ser, Ala, Gly), while no known human proteases recognize this cleavage site [2, 3]. 3CLpro can thus be considered a highly attractive drug target for the development of SARS-CoV-2 antivirals [4]. The potential of 3CLpro inhibitors has become apparent with the development of nirmatrelvir (PF-07321332), a peptidomimetic reversible covalent inhibitor that is co-formulated with the pharmacokinetic enhancer ritonavir (the resulting combination being marketed as Paxlovid) [5]. When treatment is initiated during the first days after symptom onset, it results in substantial clinical benefit [6-9]. We recently demonstrated that nirmatrelvir is equipotent *in vitro* against the current SARS-CoV-2 variants of concern (VoC). Nirmatrelvir protects Syrian Golden hamsters from intranasal infection with different VoCs and prevents transmission to untreated co-housed sentinels [10, 11]. Other clinical candidate 3CLpro inhibitors include ensitrelvir (S-217622), a non-peptidic, non-covalent SARS-CoV-2 3CLpro inhibitor[12, 13], and PBI-0451 [14]. The clinical development of lufotrelvir, an intravenous pro-drug of PF-00835321 has been discontinued [15, 16].

Treatment with antivirals can result in the selection of resistant viral variants and subsequent therapeutic failure. This has been described extensively in the treatment of (chronic/persistent or acute) viral infections caused by HIV, HBV, HCV, herpesviruses or influenza [17, 18]. Importantly, transmission of resistant viruses has been reported for HIV and influenza [19, 20]. For SARS-CoV-2, selection of resistant isolates has only been described for remdesivir, a polymerase inhibitor. *In vitro* selection with remdesivir results in the emergence of resistance-associated mutations. Yet, in the clinical setting, treatment with remdesivir so far only led to the selection of mutations that are associated with low level resistance [21-23]. A causal effect between SARS-CoV-2 resistance to any replicase inhibitors and therapy failure has not yet been demonstrated, most likely because these inhibitors are not yet widely used in the clinic and/or resistant variants might have a fitness disadvantage.

Here we report on a pathway by which SARS-CoV-2 achieves significant resistance and cross-resistance to 3CLpro inhibitors during serial passage in cell culture in the presence of a first generation 3CLpro inhibitor, ALG-097161. This molecule was prepared as a tool compound in the context of a drug discovery program.

Results

SARS-CoV-2 acquires resistance to 3CLpro Inhibitors during passage with ALG-097161

ALG-097161 is a SARS-CoV-2 inhibitor with an EC_{50} of 0.59 µM when tested for inhibition of SARS-CoV-2 isolate GHB-0302, a prototypic Wuhan isolated from a Belgian patient, in VeroE6 cells (Table 1). It has no effect on the viability of uninfected host cells at concentrations up to 10 µM. Since VeroE6 cells have a high efflux of some chemotypes, all selection experiments, antiviral assays and toxicity assays on these cells were performed in the presence of the P-glycoprotein (Pgp) efflux inhibitor CP-100356 (0.5 µM) [24]. The antiviral activity of ALG-097161 can be ascribed to inhibition of 3CLpro (IC_{50} = 0.014 µM - Table 4) and there is no relevant inhibitory effect on human Cathepsin L (IC_{50} > 10 µM – Supplemental S1). For comparative reasons, the chemical structures of ALG-097161 and the clinical 3CLpro inhibitors nirmatrelvir, PF-00835231 and ensitrelvir are shown in Figure 1.

To identify resistance development to 3CLpro inhibitors, we passaged SARS-CoV-2-GHB-0302 in VeroE6 cells in the presence of increasing concentrations of ALG-097161. The selection started at a concentration of 0.4 µM and for each next passage the virus was cultured at the same concentration, a 3x higher concentration and a 3x lower concentration. The culture demonstrating virus breakthrough, as observed by a significant cytopathic effect, at the highest concentration was then used for the next passage. We started this experiment in triplicate but for two trials we could not significantly increase the ALG-097161 concentration above 2 µM by passage 8. These cultures were therefore not further analyzed. In one culture however, the concentration of ALG-097161 could be increased gradually to 5 µM at passage 8 (p8, day 28) (Figure 2) and maintained for one passage at 15 µM, but that concentration had to be decreased again to 5 µM for the subsequent passages to allow viral replication until p12 (day 39) (Figure 2). Whole genome sequencing (Illumina) was performed on RNA purified from harvested supernatant at passages 5, 8 and 12. At p5, no mutations were identified in the 3CLpro gene but at p8 and p12 dominant mutations (>80% of the reads) were present that result in amino acid substitutions L50F E166A and L50F E166A L167F, respectively (Figure 2; Supplemental S2). As a control, SARS-CoV-2 was also passaged, at the same frequency, in the absence of compound and no mutations were identified in the 3CLpro gene at any passage (data not shown).

Analysis of the full genome of the selected viruses shows that also other nonsynonymous mutations became fixed (Supplemental S2). This can be explained by the fact that the nucleotide changes, resulting in the 3CLpro substitutions, occurred in a minor variant that also had these background mutations. Importantly, all these other changes are outside of the 3CLpro gene or the 3CLpro cleavage sites encoding sequences (Supplemental S2).

For phenotypic analysis, a new virus stock (p13) was grown in the presence of 4 µM ALG-097161, and the presence of L50F E166A L167F was confirmed by genotypic analysis. Antiviral testing with this stock showed strong resistance to ALG-097161 and cross-resistance to both nirmatrelvir and PF-00835231 (Table 1). The EC_{50} values for all these 3CLpro inhibitors are increased > 10x. As expected, the sensitivity for the polymerase inhibitor remdesivir remains unchanged.

142 In a second series of experiments, we investigated whether the observed amino acid
143 substitutions in 3CLpro are sufficient for the resistance phenotype. To this end, we engineered,
144 using an infectious clone [25], virus stocks with L50F, E166A L167F or L50F E166A L167F.
145 Unfortunately, we were not able to generate virus with E166A or L167F alone. Genotypic analysis
146 confirmed the presence of the mutations and revealed that there were no other nonsynonymous
147 mutations (data not shown). Antiviral testing with these engineered viruses shows that L50F by
148 itself is not associated with resistance while E166A L167F and L50F E166A L167F cause a 4.6x and
149 10.3x increase in EC_{50} for ALG-097161, respectively (Table 2). Again, cross-resistance is detected
150 for nirmatrelvir (EC_{50} increased 29x with the L50F E166A L167F virus). At this stage of our study,
151 ensitrelvir became available; we found that also this molecule shows cross-resistance (EC_{50}
152 increased 44x with L50F E166A L167F). For all protease inhibitors tested we observe less
153 resistance with the E166A L167F virus as compared with the L50F E166A L167F virus. Importantly,
154 all the viruses analyzed remained fully sensitive to remdesivir.
155

156 Resistance to 3CLpro inhibitors in a cell-based reporter assay

157 The resistance profile was next confirmed in a previously described cell-based reporter assay of
158 SARS-CoV-2 3CLpro enzymatic function [26]. In this gain-of-signal assay, inhibition of 3CLpro
159 results in an increased eGFP signal. Introducing the three amino acid changes L50F E166A L167F
160 into the construct resulted in a 23x and 28x loss of potency for ALG-097161 and nirmatrelvir
161 respectively (Table *3*). The resistance level of the triple mutant against PF-00835231 was 6.9x.
162

163 Effect of amino acid substitutions on 3CLpro enzymatic activity

164 Recombinant 3CLpro proteins were produced with the L50F, E166A and L167F substitutions alone
165 or combined, and their enzymatic activity was tested in a FRET assay using a peptide substrate
166 featuring the canonical glutamine cleavage site [27]. In this assay, wild-type (WT) 3CLpro shows
167 linear product conversion in the enzyme concentration range of 0.5-12.5 nM (Figure 3A).
168 Compared with the WT protein, all tested mutants display reduced enzymatic activity (Figure 3B).
169 The E166A and L167F, as single mutants, reduce the activity to about 12-20% of wild-type,
170 whereas the L50F substitution reduces the activity to as low as 0.4%. The enzyme containing the
171 three substitutions L50F E166A L167F is less compromised than L50F alone, with 4.6% activity as
172 compared with WT. The loss in enzymatic activity for each mutant might be attributed to an
173 apparent reduced binding affinity for the substrate, a loss in protein stability and/or a reduced
174 formation of active dimers (Figure 4). The enzymes with E166A and L167F are less impaired than
175 the enzyme with L50F. In comparison, the triple mutant exhibits an intermediate phenotype for
176 both parameters (Figure 4).
177 Ligand-induced protease activation and dimerization with low concentration of active site
178 inhibitor has previously been described for MERS 3CLpro [28]. This is explained by the inhibitor
179 stabilizing dimer formation by occupying only one of the two binding sites, while full occupancy
180 of the two dimer active sites results in complete enzyme inhibition (Figure 5B). Although we did
181 not perform direct protein dimerization studies, we could demonstrate that the impaired
182 enzymatic activity of the mutants can be partially rescued with low concentrations (around 0.05
183 µM) of ALG-097161, PF-00835231 or nirmatrelvir, while higher concentrations inhibit product
184 formation (Figure 5A; Supplemental S3).

Resistance to 3CLpro inhibitors in the biochemical assay

Based on the characterization of the different enzymes (see above), we decided to use all enzymes at a concentration of 50 nM to quantify the activity of the inhibitors. The effect of the L50F substitution could not be determined under these conditions due to its low intrinsic enzymatic activity. ALG-097161, nirmatrelvir and PF-00835231 all inhibit WT 3CLpro with IC_{50} values ranging from 13-23 nM (Table 4). For ALG-097161, the IC_{50} increases 5x-6x with single substitutions E166A and L167F, and reaches 35x for the enzyme with L50F E166A L167F. In comparison, the potency of nirmatrelvir is more affected by substitution E166A vs. L167F (10x vs. 4.4x) and reaches 72x increase on the enzyme with the 3 substitutions. For PF-00835231, the shift in IC_{50} is in general lower with a 6.0x change vs. the enzyme with L50F E166A L167F. However, the shift in IC_{50} is higher (~100x) with the non-covalent and chemically distinct inhibitor ensitrelvir.

Structural Biology and Computational Chemistry

Experimental data with the 3CLpro system and computational chemistry investigations were used to rationalize the phenotype observed for ALG-097161 *in vitro*.

PF-00835231 and the associated crystal structure 6xhm provided a convenient starting point for modeling ALG-097161 in the catalytic pocket of 3CLpro, due to the structural similarity between both compounds. In particular, both structures feature a hydroxymethyl-ketone warhead that binds covalently to Cys145, as well as a 4-methoxyindole-P3 substituent.

Multiple conformations of ALG-097161 were used as input for docking calculations. These yielded a well-converged predicted binding mode of ALG-097161 covalently bound to the catalytic site of WT 3CLpro (Figure 6). In line with the crystal structures disclosed for similar compounds (e.g., 6xhm), ALG-097161 is predicted to form a covalent bond from the activated carbon atom of its hydroxymethyl-ketone warhead to the side chain of the catalytic C145 residue, anchoring the inhibitor into the binding cleft of 3CLpro. ALG-097161 forms seven direct hydrogen bonds with the SARS CoV2 3CLpro catalytic site. The oxygen atom of the inhibitor's warhead interacts with the backbone NH of C145 in the oxyanion hole. The carbonyl oxygen of the P1 lactam hydrogen-bonds to the side chain of H163, while the NH of the P1 lactam is involved in a bifurcated interaction with the side chain of E166 and the backbone carbonyl of F140. The peptide backbone of ALG-097161 anchors itself with hydrogen bonds to the backbone carbonyl of H164 and the backbone HN of E166. The NH function of the P3 indole hydrogen-bonds the inhibitor to the backbone carbonyl of E166. The fused bicyclic P2 substituent of ALG-097161 maximizes Van der Waals interactions via extensive productive contacts to the protein side chains that form the S2 sub-pocket of WT 3CLpro. A key difference with PF-00835231 resides in the (lack of) interaction between the inhibitor backbone and Gln189; a direct consequence of the cyclization on P2, which results in the loss of a hydrogen bond donor site.

224 The predicted binding mode of ALG-097161 within 3CLpro provides some rationale for the amino
225 acid substitutions associated with resistance. In particular, residues 166 and 167 are located
226 within 5Å of the bound ALG-097161. This observation can be extended to both PF-00835231 and
227 nirmatrelvir, based on crystal structures from PDB codes 6xhm and 7rfw, respectively.
228 Consequently, the observed substitutions have a direct impact on the compound / target
229 interaction.

230 E166 plays a key role in compound binding, with no less than three hydrogen bonds formed with
231 the inhibitors. The E166A substitution eliminates one of the hydrogen bonds made within the P1
232 sub-pocket. Interactions with this sub-pocket are important for substrate recognition by
233 coronaviral 3CLpro enzymes, and its occupancy, in many cases by a lactam moiety, is a key driver
234 for inhibitor potency. It is therefore unsurprising that all three inhibitors are adversely affected
235 by the E166A change. Meanwhile, L167F results in the presence of a bulkier side chain on the
236 neighboring position. While this change does not directly conflict with compound binding, the
237 side chain of L167 is in close contact with other residues, including Phe185. Molecular Dynamics
238 (MD) simulations on the L50F E166A L167F enzyme suggest that the bulkier Phe side chain results
239 in some distortion of the neighboring sub-pocket. In particular, the loop containing L167F moves
240 away from F185 and the distance between the Cαs of F185 and L167F / P168 consistently
241 increases, resulting in a more open binding site and a sub-optimal fit of the inhibitor, even though
242 H-bond interactions (including the two remaining H-bonds with the A166 backbone) appear
243 conserved throughout 100ns simulations (Figure *7*). Interestingly, all three inhibitors (ALG-
244 097161, PF-00835231 or nirmatrelvir) were affected by the L167F change.

245 Reasons behind the L50F mutation remain more elusive, as this residue falls outside of direct Van
246 der Waals or hydrogen-bond contact range to ALG-097161. However, the L50 side chain is located
247 only 2.7 Å from Q189, a residue which can interact with the peptide backbone of this inhibitor
248 class either directly (as with PF-00835231) or *via* water molecules. L50F might therefore indirectly
249 affect compound binding by altering the position of Q189 and the subsequent interactions
250 mediated by this residue. However, a rigorous assessment of how this change impacts enzyme
251 activity and/or inhibitor binding would require more elaborated techniques (e.g., free energy
252 perturbation) that are beyond the purpose of this work.

253 Finally, it is anticipated that the natural SARS CoV-2 polyprotein substrates, that are processed
254 by the 3CLpro, are less affected by the L50F, E166A and/or L167F substitutions, due to their larger
255 size and approximately two-fold higher number of polar interactions with the protease (as
256 observed in 2q6g.pdb for SARS CoV-1 3CLpro in complex with bound substrate).

257

Discussion

Nirmatrelvir is the first oral SARS-CoV-2 (3CLpro) protease inhibitor granted emergency use authorization by the US FDA for the treatment of COVID-19. To avoid resistance development, HIV and HCV protease inhibitors are used, with great success, in fixed dose combinations with other directly acting antiviral drugs that have a different mechanism of action [29]. As a single agent, several of these inhibitors select (rapidly) for drug-resistant variants. SARS-CoV-2 infections are typically acute in nature; hence treatment can be of short duration, which may largely reduce the likelihood that resistant variants develop. Yet, also for acute infections, the emergence of drug-resistant variants is a serious concern, certainly in case that such variants can efficiently transmit resulting in a loss of therapeutic options for patients. For example, the first-generation influenza drugs, amantadanes, are no longer recommended, as resistance to amantadine and rimantadine is widespread [20].

To monitor clinical drug-resistance, it is crucial to identify the mutations involved. To that end, we used the 3CLpro inhibitor ALG-097161, a probe compound in the context of a drug discovery program, to select for resistant variants *in vitro* by passaging SARS-CoV-2 in presence of increasing drug concentrations. Similar experiments have been performed with SARS-CoV-2 neutralizing antibodies and polymerase inhibitors [22, 30].

The selection process indicated that there is a significant barrier to resistance for the 3CLpro inhibitor ALG-097161. The first changes were observed only between passage 5 and 8 (20-30 days). These were the double substitution L50F E166A in 3CLpro, which then evolved to the triple substitution L50F E166A L167F. Phenotyping this triple mutant virus revealed a 63x increase in the EC_{50} for ALG-097161. Moreover, significant cross-resistance (>10x increase EC_{50}) was observed with nirmatrelvir, the active component of Paxlovid, and PF-00835231, an earlier 3CLpro clinical candidate. Next, we engineered an infectious clone with the only the 3CLpro substitutions L50F E166A L167F and the resistance against ALG-097161, nirmatrelvir and also ensitrelvir could be confirmed (>10x increase EC_{50}). As a second confirmation, a cell-based assay was used with heterologous expression of wild-type and mutated 3CLpro (L50F E166A L167F) and a substrate linked to a reporter protein. The EC_{50} values for ALG-097161 and nirmatrelvir in this assay increase 23x and 28x respectively as compared with wild-type. Importantly, all of the viruses analyzed remained fully susceptible to the polymerase inhibitor remdesivir (GS-441524 form).

We further characterized the 3CLpro substitutions using biochemical assays. Enzymes carrying the single substitution L50F, E166A or L167F were found to have markedly lower enzymatic activity (<20% as compared to wild-type). In particular, the L50F mutant enzyme had only 0.4% activity compared to wild-type, which could be restored to 4.6% when also E166A and L167F were introduced. Each of the enzymes was also less efficiently inhibited by the 3CLpro inhibitors. The largest increase in IC_{50} was observed when all three substitutions L50F E166A L167F were combined. For this triple-mutant enzyme, the IC_{50} for ALG-097161, nirmatrelvir and ensitrelvir increases by 35x, 72x and 93x respectively.

A structural biology analysis reveals that the substitutions decrease interactions between the enzyme and the inhibitor. E166A causes a direct loss of a hydrogen bond with the lactam-moiety that is found in all the inhibitors tested here, L167F increases the size of the binding pocket

301 causing a decrease of the Van der Waals forces between enzyme and inhibitor, and L50F is
302 thought to change the rotamer conformation of Q189, which, for the wild-type, has many
303 interactions with the inhibitors through a network of water molecules.
304 The loss of interactions, resulting from amino acid substitutions associated with resistance, might
305 have a lower effect on substrates than on inhibitors, as the former rely on a significantly higher
306 number of interactions for binding. Consequently, these resistance-associated mutations seem
307 to allow a better discrimination between substrate and inhibitor at the expense of intrinsic
308 enzymatic activity.
309 A recent sequence analysis across 4.9 million global SARS-CoV-2 isolates, circulating prior to the
310 introduction of Paxlovid, showed a high genetic conservation of the 3CLpro protein [31]. From
311 the 305 amino acid positions, only 3 have a polymorphism in >1% of the samples and 13 have a
312 change in 1% - 0.11% of the samples. Changes at positions L50, E166 or L167 have a <0.11%
313 prevalence. E166 displays extreme high conservation in this dataset with <0.001% samples having
314 an alternative amino acid.
315 At this moment, peer-reviewed information on resistance against 3CLpro inhibitors in COVID-19
316 patients is, to our knowledge, not available. The Paxlovid label indicates that E166V is more
317 common in nirmatrelvir/ritonavir-treated subjects relative to placebo-treated subjects (0.8% and
318 <0.2% respectively), and in one patient, with a baseline L50F substitution, the E166V substitution
319 co-occurred with L50F on Day 5 of treatment [32]. Both these observations are in accordance
320 with the results described above.
321 While we can clearly observe resistance of different 3CLpro inhibitors for the L50F E166A L167V
322 virus, we could not fully characterize the contribution of each substitution by itself. During the
323 selection experiment, L50F together with E166A is selected first and L167V is acquired later.
324 Additional cell-based experiments demonstrate that an L50F carrying virus is not resistant, while
325 biochemical experiments indicate that E166A and L167F are associated with resistance. Taken
326 together, we hypothesize that E166A is the main driver for resistance, that L50F is needed to
327 support E166A and that presence of L167F further increases resistance. It would require an
328 extensive study of the replication capacity of the different variants to support this hypothesis.
329 Importantly, clear nirmatrelvir/ensitrelvir cross-resistance is observed with both the E166A L167F
330 and L50F E166A L167F viruses.
331 During the writing of this manuscript, two preprints reported the selection of nirmatrelvir
332 resistant SARS-CoV-2 viruses. One group performed > 480 independent selection experiments,
333 resulting in the identification of multiple pathways of nirmatrelvir resistance [33]. They conclude
334 that E166V confers the highest level of resistance of all substitutions tested (100x for nirmatrelvir;
335 23x for ensitrelvir). In addition, these authors show that E166V causes a reduced fitness that is
336 restored by adding L50F or T21I. The selection of L50F E166V by nirmatrelvir *in vitro* has also been
337 reported by another group [34]. Also, these authors come to the conclusion that E166V is
338 responsible for resistance whereas L50F is a compensatory substitution required for maintaining
339 fitness. As E166A and E166V are very similar substitutions (alanine and valine have similar
340 chemical structures), these findings are in strong agreement with our observations. A third group
341 engineered a chimeric VSV-variant, that has SARS-CoV-2 3CLpro expressed in an artificial
342 polyprotein, for which the replication depends on 3CLpro activity. Selection for nirmatrelvir
343 resistance resulted in the appearance of L167F in the absence of other mutations, and an

344 engineered SARS-CoV-2 infectious clone with only the L167F substitution showed a marginal level
345 of resistance for nirmatrelvir (2x increase EC_{50})[35].
346 Important to mention is also the work of Flynn et al [36], who performed different functional
347 3CLpro screens in yeast to study the resilience of all amino acid positions towards substitutions.
348 Interestingly, the authors conclude that position E166 is highly tolerant to substitutions including
349 the E166A or E166V substitution. Based on available structural biology data of 3CLpro in complex
350 with inhibitors or natural substrate and the functional screen data, these authors identified
351 E166A and E166Q as potentially resistance associated substitutions.
352 Our report emphasizes the need for additional research to elucidate potential resistance
353 pathways of SARS-CoV-2 inhibitors *in vitro*. It is also a starting point for the surveillance of
354 nirmatrelvir resistance and indicates the potential need for combination therapies with different
355 classes of SARS-CoV-2 inhibitors.
356

Methods

Compounds, cells, viruses, proteins and peptides

ALG-097161, Nirmatrelvir and PF-00835231 were synthesized by Aligos Therapeutics and purified to >95% purity. GS-441524 was obtained from MedChem Express (cat no HY-103586). The African green monkey kidney Vero E6 cell line was purchased from ATCC (catalog no. CRL-1586™) and maintained in DMEM (gibco cat no 41965-039) supplemented with 10% v/v heat-inactivated FCS. The SARS-CoV-2 GHB-03021 (EPI ISL407976|2020-02-03) isolate was obtained from a Belgian patient returning from Wuhan in February 2020. The isolate was passaged 7 times on VeroE6 cells, which introduced two series of amino acid deletions in the spike protein [37].
SARS-CoV-2 3CLpro wild-type and mutant enzymes were produced as previously described [38]. Peptide substrate (Dabcyl-KTSAVLQSGFRKM-E(Edans)-NH_2 for FRET was sourced from Biopeptide (San Diego, CA) at >95% purity.

Genotypic analysis

Illumina sequencing

RNA was extracted from cell culture supernatant, using the NucleoSpin RNA virus kit (Macherey-Nagel) according to the manufacturer's instructions. Whole genome sequencing was outsourced to EurofinsGenomics (ARTIC SARS-CoV-2 WGS, Konstanz, Germany), who performed reverse transcription, enrichment of the viral genome using a primer set similar to the ARTIC primers (> 200 primer pairs, covering the full 29.9 kb viral genome), generation of libraries, Illumina sequencing (2x150 bp read mode), and sequence cleaning to remove adapters and poor-quality bases. Sequences were further analyzed using Geneious Prime software (v2022.2.1) by mapping to the SARS-CoV-2 RefSeq NC_045512, and variant calling as described by the software manufacturer (https://help.geneious.com/hc/en-us/articles/360045070991-Assembly-of-SARS-CoV-2-genomes-from-tiled-amplicon-Illumina-sequencing-using-Geneious-Prime). For each sample, >0.9 M reads that could be aligned with the SARS-CoV-2 genome were obtained with >99.5% of untrimmed bases being of high-quality, and a mean coverage of > 4000 reads.

Oxford Nanopore sequencing

As a control, the same samples were also sequenced using an inhouse pipeline. For this Reverse transcription was carried out via SuperScript IV and cDNA was posteriorly amplified using Q5® High-Fidelity DNA Polymerase (NEB) with the ARTIC nCov-2019 primers, following the recommendations in the sequencing protocol of the ARTIC Network (https://artic.network/ncov-2019). Samples were multiplexed following the manufacturer's recommendations, using the Oxford Nanopore Native Barcoding Expansion kits NBD104 (1-12) and NBD114 (13-24), in conjunction with Ligation Sequencing Kit 109 (Oxford Nanopore). Sequencing was carried out on a MinION sequencer using R9.4.1 flow cells and MinKNOW 2.0 software. Both methods resulted in the same consensus sequence for each sample. For further mutation analysis we used the deep sequencing data generated by the Illumina protocol.

398 ## Antiviral testing

399 The 50% effective concentration (EC_{50}), the concentration of compound required for fifty percent
400 antiviral activity, was determined on VeroE6 cells as follows. On day -1, the test compounds were
401 serially diluted in 100 µL assay medium (DMEM supplemented with 2% v/v FCS) in 96-well plates.
402 In a next step, 50 µL of VeroE6 cells (25,000 cells/well) was added together with 2 µM of the
403 MDR1-inhibitor CP-100356 (final concentration 0.5 µM). The plates were incubated (37°C, 5%
404 CO2 and 95% relative humidity) overnight. On day 0, 50 µL of SARS-CoV-2 WT or the triple mutant
405 strain at a multiplicity of infection (MOI) of 0.001 tissue culture infectious dose (TCID50) per cell
406 was added and the plates were stored in a humidified incubator at 37°C and 5% CO2. In absence
407 of antiviral activity, the VeroE6 cells undergo a cytopathic effect. Cell viability was determined 4
408 days p.i. using a viability staining with MTS [39]. The percentage of antiviral activity was
409 calculated by subtracting background and normalizing to the untreated-uninfected control wells,
410 and the EC_{50} was determined using logarithmic interpolation.
411

412 ## Generation and rescue of recombinant viruses

413 We used the in-yeast transformation-associated recombination (TAR) cloning method as
414 described previously with some adaptations [25]. In sum, the whole SARS-CoV-2 genome was
415 encoded in 12 overlapping DNA fragments. These so-called WU-Fragments and a TAR-vector are
416 homologous recombined in yeast forming the yeast artificial chromosome (YAC). The SARS-CoV-
417 2 3CLpro is encoded on WU-Fragment 5 and was replaced with newly generated and overlapping
418 PCR products to introduce the amino acid changes L50F, E166A L167F or L50F E166A L167F. The
419 overlapping PCR products were made via reverse transcription from RNA purified from vRNA of
420 the virus stock obtained from the selection. In brief, cDNA was generated from RNA by LunaScript
421 RT SuperMix (NEB). PCR reactions targeting the 3CLpro gene were performed using Q5® High-
422 Fidelity DNA Polymerase (NEB) and the resulting PCR products were mixed and matched to
423 recombine SARSCoV-2 3CLpro^{L50F} , SARSCoV-2 3CLpro$^{E166A\ L167F}$ and SARSCoV-2 3CLpro$^{L50F\ E166A}$
424 ^{L167F}. All PCR products were purified with the High Pure PCR Product Purification Kit (Roche)
425 before being used for TAR cloning.
426 In vitro transcription was performed for EagI-cleaved YACs and PCR-amplified SARS-CoV-2 N gene
427 using the T7 RiboMAX Large Scale RNA production system (Promega) as described previously
428 [25]. Transcribed capped mRNA was electroporated into baby hamster kidney (BHK-21) cells
429 expressing SARS-CoV N protein. Electroporated cells were co-cultured with susceptible Vero
430 TMPRSS2 cells to produce passage 0 (P.0) of the recombinant viruses. Passage 1 virus stocks were
431 further produced in Vero TMPRSS2 cells and the presence of mutations was confirmed by
432 Illumina sequencing. These results also showed the absence of other non-synonymous mutations
433 in the viral genome.
434

435 ## 3CLpro FRET-based assay

436 The FRET-based assay was performed similarly to the SAMDI-MS assay. Assays were performed
437 in 20 µL volume in 384-well Non-binding Low-volume plates (Greiner Bio-One; Monroe, NC) at
438 ambient temperature. 3CLpro and its mutants were preincubated with inhibitors for 30 min.
439 Reactions were initiated by the addition of a FRET-compatible peptide substrate Dabcyl-
440 KTSAVLQSGFRKM-E(Edans)-NH_2. Fluorescence was measured for 90 minutes at 2-min intervals

441 using a 340/460 excitation/emission filters on a Envision plate reader (Perkin Elmer). The IC_{50}
442 values were calculated by fitting the curves using a four-parameter equation in GraphPad Prism.
443 To calculate the dimer dissociation constant (K_d), the velocities of enzyme titration of WT and
444 mutant 3CLpros were fitted to the equations (1) and (2).
445 $V_0=V_{max}[S]/(Km+[S])$ (1)
446 $V_{max} = K_{cat}[D] = K_{cat}\frac{K_d+4C_T-\sqrt{K_d{}^2+8K_dC_T}}{8}$ (2)
447 Equation (2) was described previously for the calculation of monomer dimer equilibrium
448 dissociation constant (K_d) [28].
449

450 ## 3CLpro cell-based reporter assay

451 The cell-based reporter assay of SARS-CoV-2 3CLpro enzymatic function was described previously
452 [26]. This gain-of-signal assay is based on the expression of a chimeric protein consisting of Src-
453 Mpro-Tat-eGFP in which the Mpro amino acid sequence is flanked with cognate N- and C-terminal
454 self-cleavage sites. While it was expected that Mpro inhibition would result in a different
455 subcellular localization of the GFP signal, it was found that without Mpro inhibition there is no
456 detectable GFP expression, while in the presence of Mpro inhibition there is high GFP expression.
457 Hence the naming gain-of-signal assay. The exact mechanism behind this reporter system is not
458 known but results suggest a mechanism in which Mpro activity somehow suppresses the
459 accumulation of reporter mRNA in transfected cells.
460 293T cells were maintained at 37°C/5% CO2 in Dulbecco's DMEM (Corning#10-013-CV)
461 supplemented with 10% fetal bovine serum (Gibco #10091148) and 1% penicillin/streptomycin
462 (Gibco #15140122). 293T cells were seeded in a 96-well plate at 5×10^5 cells/well and returned to
463 incubation for 24h. The following day, cells were treated with compound at a final DMSO
464 concentration of 2% prior to transfection with 100 ng of the wild-type or triple mutant (L50F
465 E166A L167F) plasmid with Lipofectamine LTX (ThermoFisher#15338100) for 24h. Post 24h
466 transfection, GFP fluorescence was detected with a Victor (Perkin Elmer) using the Fluorescein
467 485/535 setting. Inhibition was determined from the resulting fluorescent signal and graphed
468 using a variable slope four parameter curve fitting with GraphPad Prism (v 9.2.0).
469

470 ## Modeling of inhibitors in WT and mutant (L50F E166A L167F) 3CLpro

471 PDB structure 6xhm (complex with PF-00835231) was used as starting point for modeling
472 compounds in WT and mutant (L50F E166A L167F) 3CLpro. The receptor structure was cleaned
473 up and minimized with restraints ahead of docking using the Protein Preparation Wizard in
474 maestro (Schrödinger). Ligands were processed using the Ligprep module in maestro.
475 Stereoisomers were not generated, as the absolute configuration of the ligand was known.

476 Covalent docking was used to predict the binding mode of ALG-097161. C145 was specified as
477 the reactive residue for covalent binding, and the centroid of the X-ray reference ligand was used
478 to define the investigated binding site. A custom covalent reaction parameter file was used to
479 define the reaction between the warhead moiety and the catalytic C145. High accuracy (Pose
480 Prediction Thorough) docking methodology was implemented for pose prediction. Initial docking
481 poses within 4 kcal/mole (glide gscore) were collected for further processing. Residues within 6

Å of the bound compound were minimized after covalent bond formation. The top 5 binding mode suggestions were saved for visual inspection.

Initial structures for the L50F E166A L167F triple mutant were built by introducing the mutations directly into the WT complex. An initial restrained minimization was done with the protein preparation wizard to remove any unacceptable clash. Next, a Desmond simulation system was built (see below) and a 100 ps energy minimization procedure was run with Desmond to reach the nearest energy minimum.

Molecular Dynamics (MD) simulations were performed using the Desmond-GPU package. A simulation system was first set up around the protein-inhibitor complex, including a 10 Å water box, Na+ ions necessary to neutralize the system and additional Na+ and Cl- ions to simulate a 0.15 M NaCl concentration. OPLS4 was selected as force field. The NPT ensemble (T = 300K, P = 1.01325 bar) was used. The system was relaxed prior to simulation. MD were run for a (simulated) period of 100 ns, with frames saved every 0.25 ns (total 400 frames). Final frames were energy-minimized (100 ps minimization protocol). Protein-ligand interactions and distances were evaluated in the 5 ns - 100 ns period.

Competing interests

The authors declare the following financial interests/personal relationships which may be considered as potential competing interests. Koen Vandyck and Pierre Raboisson are employees of Aligos Belgium BV. Cheng Liu, Antitsa Stoycheva, Sarah K Stevens, Chloe De Vita, Andreas Jekle, Lawrence M Blatt, Leonid Beigelman, Julian A Symons and Jerome Deval are employees of Aligos Therapeutics, Inc. A patent application on ALG-097161 is pending

Acknowledgments

We thank Tina Van Buyten and Niels Cremers for their excellent technical assistance and Myriam Cornelis for dedicated editorial assistance.

Figures

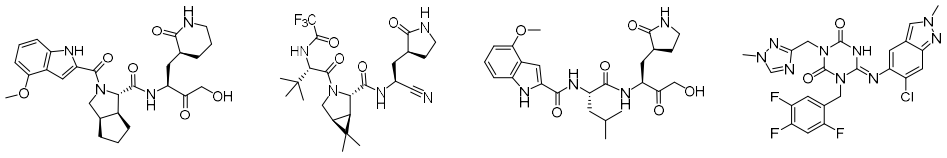

ALG-097161 | Nirmatrelvir (PF-07321332) | PF-00835231 | Ensitrelvir

Figure 1: **Chemical structures of different 3CLpro inhibitors**

518

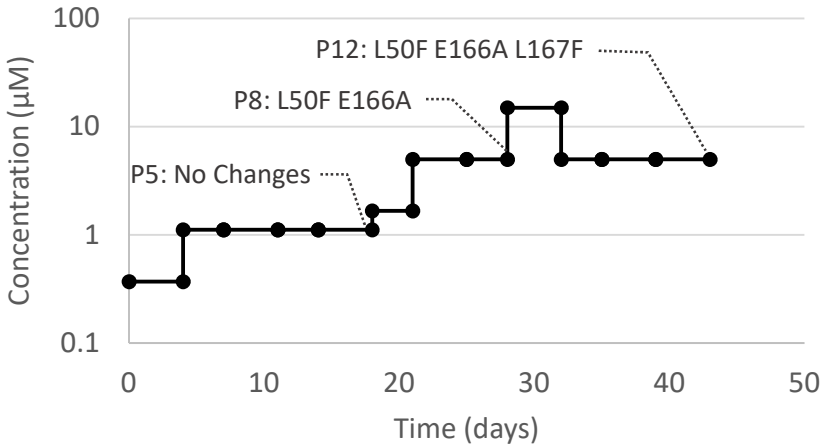

519
520 Figure 2: **Passaging SARS-CoV-2-GHB (Wuhan) in VeroE6 cells in the presence of increasing**
521 **concentrations of ALG-097161 (and the efflux inhibitor CP-100356).** Selection was initiated at
522 0.4 µM. At every passage, several new cultures were started with the same concentration as well
523 as a lower and a higher concentration. The passage with the highest compound concentration
524 that could be maintained was selected for the following passage. At passage 5, 8 and 12, vRNA in
525 the cell culture medium was sequenced. Substitutions in the 3CLpro that were found at these
526 passages are indicated.

527

528

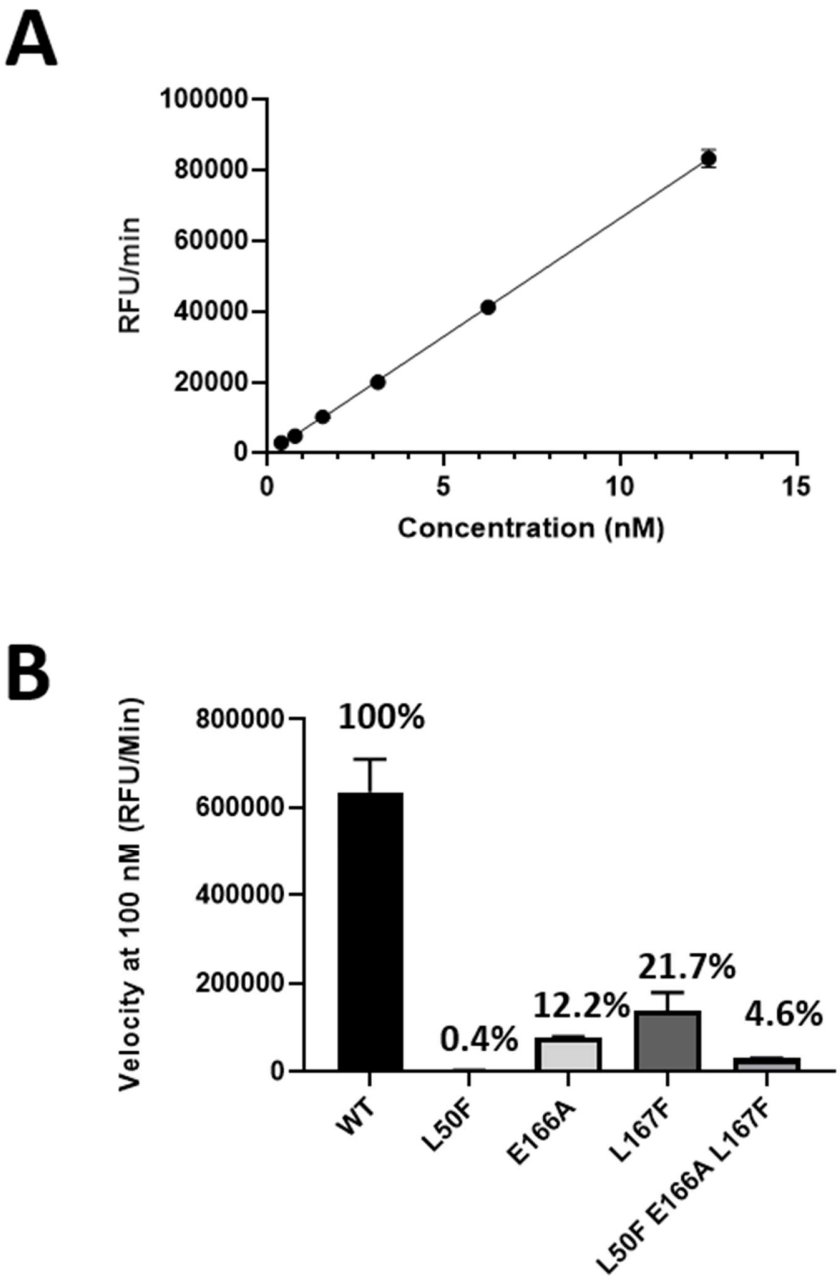

529
530 Figure 3: **Enzymatic activity of WT and mutated SARS-CoV-2 3CLpro.** (A) The enzymatic activity
531 of WT 3CLpro was measured in a FRET assay. Three independent experiments were performed.
532 The figure shows the results of one representative experiment. (B) Comparison of enzymatic
533 activity between WT 3CLpro and mutated enzymes. Each data point represents the average of
534 three independent experiments and mean and standard deviations are shown.

535

536

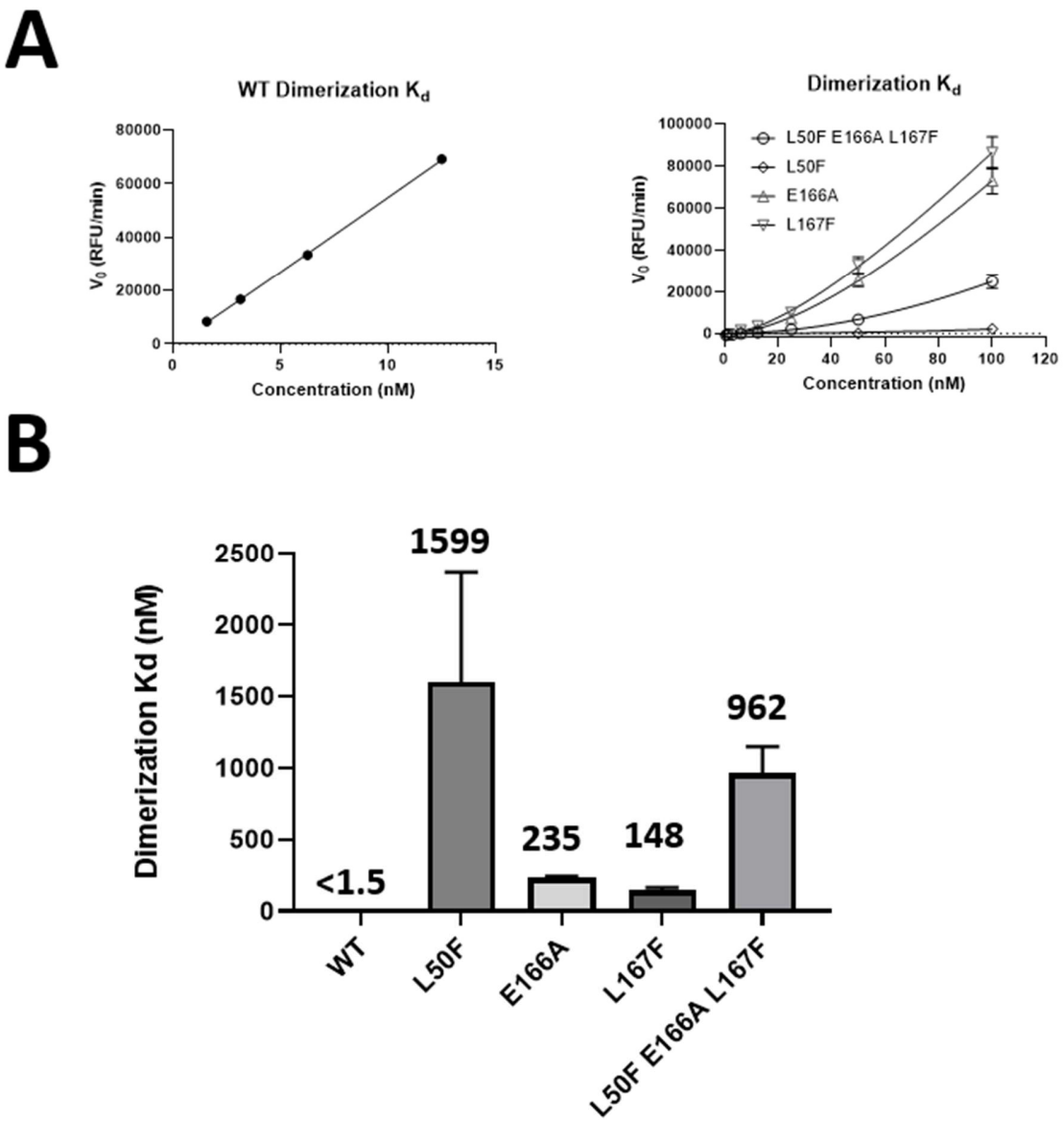

537
538 Figure 4: **Effect of mutations on 3CLpro dimerization**. (A) Initial velocities of enzyme titration of
539 3CLpro WT and mutant proteins were fitted as described (see methods) to calculate the
540 monomer dimer equilibrium dissociation constant. Three independent experiments were
541 performed. The figures show the results of one representative experiment. (B) 3CLpro
542 dimerization binding affinity for each enzyme. Each data point represents the average of three
543 independent experiments and mean and standard deviations are shown.

544
545

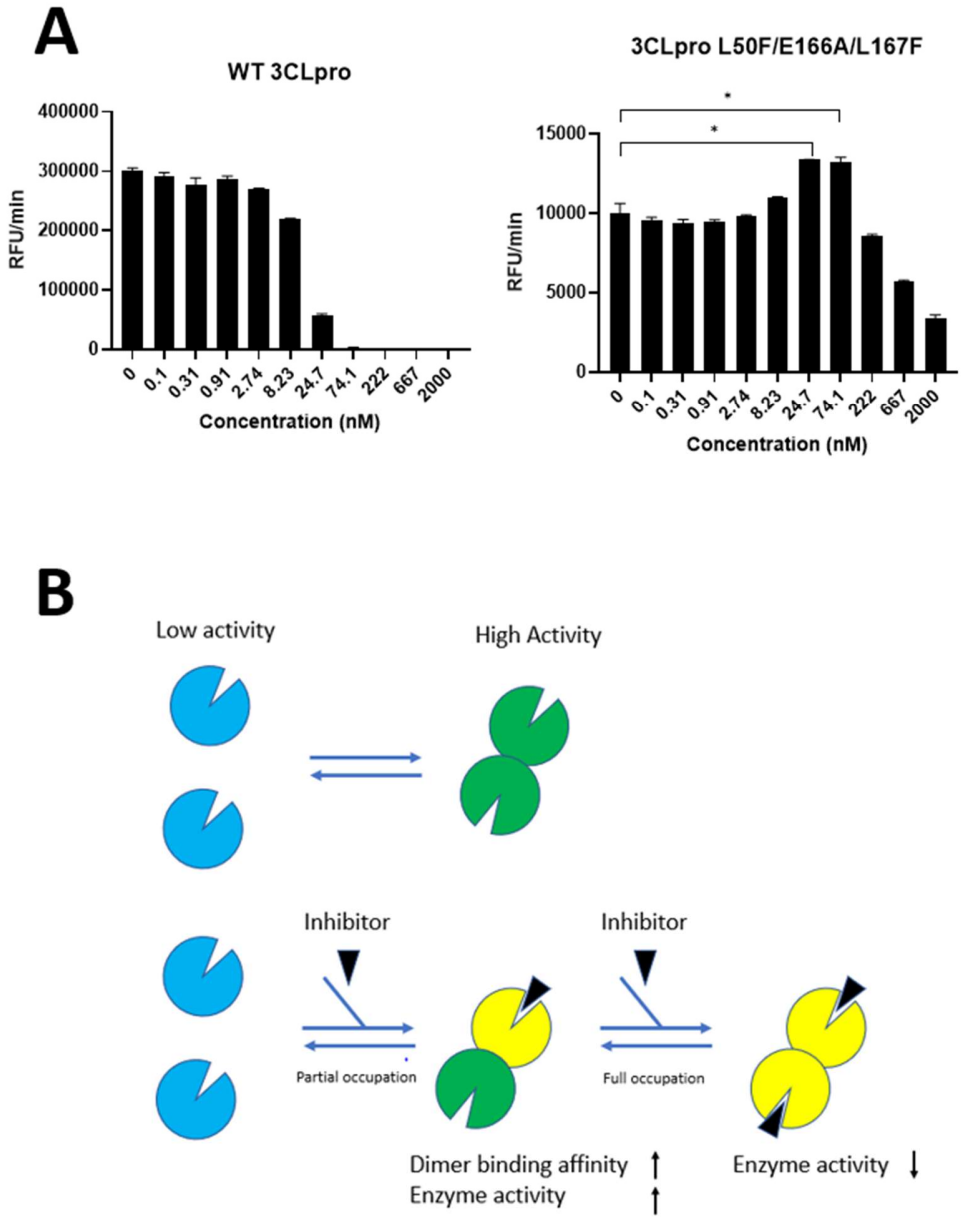

Figure 5: **Ligand-induced enzymatic activation.** (A) Comparison of ALG-097161 dose-response for WT and L50F E166A L167F 3CLpro. Three independent experiments were performed and mean and standard deviations are shown. The figure shows the results of one representative experiment. (* P< 0.05) Similar experiments with Nirmatrelvir and PF-00835231 are shown in Supplemental S3. (B) Model for ligand-induced dimerization and enzymatic activation at low concentration of inhibitor.

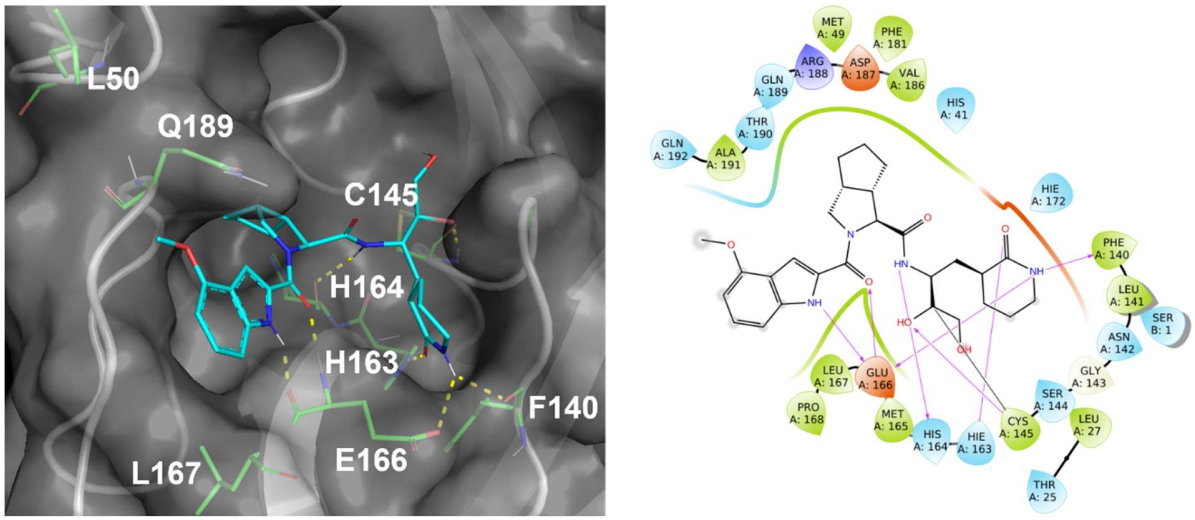

Figure 6: **Predicted binding mode of ALG-097161 covalently bound to the catalytic site of WT 3CLpro.** Left panel: ALG-097161 (carbon: cyan, nitrogen: navy; oxygen: red) covalently docked to WT 3CLpro (gray cartoon and surface; key side chains shown with carbon: green, nitrogen: navy; oxygen: red). Right panel: ALG-097161 binds covalently to the catalytic C145 and forms seven hydrogen bonds with 3CLpro: warhead to C145 in the oxyanion hole; P1 lactam to H163, E166 and F140; peptide backbone to H164 and E166; P3 indole to E166. The fused bicyclic P2 substitution maximizes Van der Waals interactions in the S2 sub-pocket.

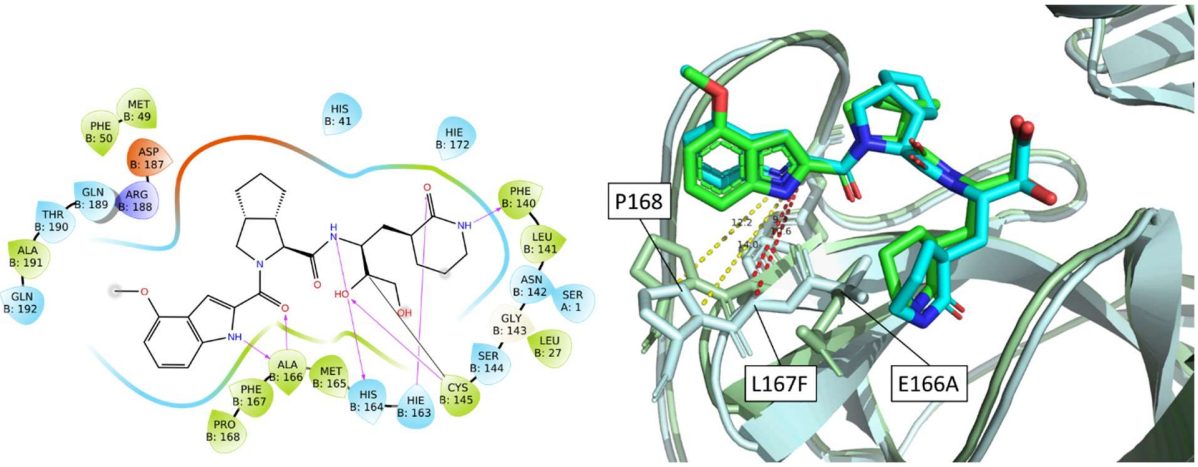

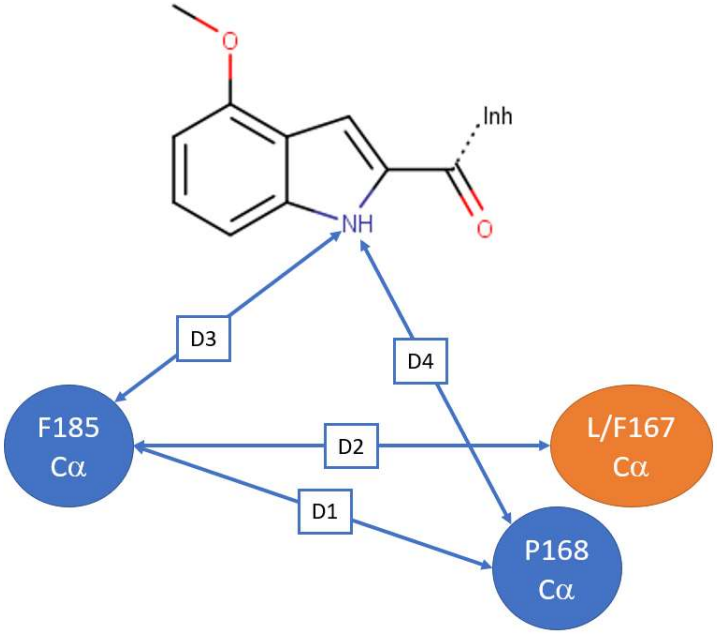

	WT (L167)	Mutant (F50,A166, F167)
D1 (Å)	12.78 ± 0.43	14.17 ± 0.59
D2 (Å)	9.70 ± 0.35	10.80 ± 0.44
D3 (Å)	10.36 ± 0.68	10.27 ± 0.44
D4 (Å)	6.47 ± 0.44	7.03 ± 0.51

Figure 7: **Proposed effect of the L167F substitution.** Accommodation of the bulkier F167 residue results in some distortion of the binding site and in a possibly sub-optimal fit. Top Left: Interaction diagram for ALG-097161 in triple-mutant (L50F, E166A, L167F) 3CLpro. Interaction between the lactam moiety and the side-chain of residue 166 is lost due to mutation, while other direct H-bond interactions are conserved (>90% occurrence) over a 100 ns MD run. Top right: Overlay of representative MD frames for WT and mutant 3CLPro. WT protein displayed as pale green cartoon and L50F E166A L167F mutant displayed as pale blue cartoon. Bottom: Average distances between F185 (Cα), L167/F167 (Cα) P168 (Cα) and inhibitor. Distances collected over 2 x 380 frames (5ns → 100ns simulated time). Distances between F185 and L/F167 + P168 are increased following the L167F change.

580 # Tables

581

582 Table 1: **Phenotypic resistance associated with the L50F E166A L167F mutation profile as**
583 **determined in VeroE6 cells**

	toxicity VeroE6 CC_{50} (µM)	**SARS-CoV-2 WT-GHB-03021 EC_{50} (µM)**	**SARS-CoV-2 L50F E166A L167F EC_{50} (µM) [FC]*** **
ALG-097161	> 10 n=4	0.59* (0.47 - 0.83)** n = 6	39 **[63]** (13 - 47) n = 6
Nirmatrelvir	> 10 n=4	0.12 (0.094 - 0.18) n = 8	6.1 **[51]** (5.8 – 8.1) n = 5
PF-00835231	> 10 n=4	0.19 (0.18 - 0.20) n = 2	4.4 **[23]** (1.0 – 7.8) n = 5
Remdesivir (GS-441524)******	> 10 n=4	0.79 (0.67 – 1.1) n = 8	1.7 **[2.1]** (0.59 – 1.9) n = 6

584

585 * Median value; ** 25th – 75th percentile, EC_{50} = 50% effective concentration, ***FC = Fold Change of EC_{50},
586 **** GS-441524 is the parent nucleoside of remdesivir, it is intracellularly converted to the same active metabolite
587 EC_{50} (50% effective concentration), CC_{50} (50% cytostatic concentration)
588 note: all assays on VeroE6 cells are performed in the presence of 0.5 µM CP-100356

589

590

591 Table 2: **Phenotypic resistance associated with the L50F, E166A L167F and L50F E166A L167F**
592 **mutation profile as determined by using reversed engineered SARS-CoV-2 viruses in the USA-**
593 **WA1 background on VeroE6 cells.**

	SARS-COV-2 WT-USA-WA1 EC_{50} (µM)	**EC_{50} (µM) [FC]***		
		L50F	**E166A L167V**	**L50F E166A L167V**
ALG-97161	0.60* (0.51-0.71)** n=4	0.98 **[1.6]** (0.83-1.1) n=4	2.9 **[4.6]** (1.5-4.5) n=4	6.2 **[10.3]** (4.8-7.3) n=4
Nirmatrelvir	0.11 (0.09-0.12) n=4	0.16 **[1.5]** (0.12-0.2) n=4	1.1 **[10.0]** (0.67-1.8) n=4	3.2 **[29]** (2.3-3.5) n=6
Ensitrelvir	0.21 (0.18-0.27) n=4	0.24 **[1.1]** (0.18-0.31) n=4	8.0 **[38]** (2.8-12.7) n=4	9.3 **[44]** (3.5-15) n=6
Remdesivir (GS-441524)****	0.86 (0.53-1.1) n=4	1.1 **[1.3]** (0.8-1.1) n=4	1.5 **[1.7]** (1.1-1.9) n=4	1.2 **[1.4]** (0.91-1.7) n=6

594 * Median value; ** 25th – 75th percentile, EC_{50} = 50% effective concentration, ***FC = Fold Change of EC_{50},
595 **** GS-441524 is the parent nucleoside of remdesivir, it is intracellularly converted to the same active metabolite
596 EC50 (50% effective concentration)
597 note: all assays on VeroE6 cells are performed in the presence of 0.5 µM CP-100356
598
599

600
601 Table 3: **Phenotypic resistance associated with the L50F E166A L167F mutation profile as**
602 **determined in a cell-based 3CLpro reporter assay**

	Wild Type EC_{50} (µM)	**L50F E166A L167F EC_{50} (µM) [FC]*** **
ALG-097161	1.7* (1.2-3.8)** n=6	39 **[23]** (10-39) n=3
Nirmatrelvir	0.96 (0.65-1.2) n=5	27 **[28]** (17-36) n=4
PF-00835231	1.6 (1.2-6.0) n=6	11 **[6.9]** (7.6-15) n=3

603 * Median value; ** 25th – 75th percentile, ***FC = Fold Change of EC50
604
605

606

607 Table 4: **Biochemical analysis of the resistance associated with different substitutions in the**
608 **3CLpro enzyme**

	Wild Type IC_{50} (nM)	**IC_{50} (nM) [FC]*** **		
		E166A	**L167F**	**L50F E166A L167F**
ALG-097161	14* (8.8-17)** n=3	77 **[5.7]** (58-90) n=3	72 **[5.3]** (55-91) n=3	480 **[35]** (220-560) n=3
Nirmatrelvir	23 (16-26) n=6	230 **[10]** (210-380) n=4	100 **[4.4]** (84-130) n=4	1600 **[72]** (820-1700) n=6
PF-00835231	13 (10-19) n=3	27 **[2.1]** (21-47) n=3	48 **[3.8]** (29-74) n=3	75 **[6.0]** (72-210) n=3
Ensitrelvir	25* (17-34)** n=3	ND	ND	2300 **[93]** (1422-3002) n=4

609 * Median value; ** 25th – 75th percentile, ***FC = Fold Change of EC_{50}, ND: not determined

610

611

612

613 # References

614

615 1. Xiong, M., et al., *What coronavirus 3C-like protease tells us: From structure, substrate*
616 *selectivity, to inhibitor design.* Med Res Rev, 2021. **41**(4): p. 1965-1998.
617 2. Fan, K., et al., *The substrate specificity of SARS coronavirus 3C-like proteinase.* Biochemical
618 and Biophysical Research Communications, 2005. **329**(3): p. 934-940.
619 3. Ullrich, S. and C. Nitsche, *The SARS-CoV-2 main protease as drug target.* Bioorg Med Chem
620 Lett, 2020. **30**(17): p. 127377.
621 4. Vandyck, K. and J. Deval, *Considerations for the discovery and development of 3-*
622 *chymotrypsin-like cysteine protease inhibitors targeting SARS-CoV-2 infection.* Curr Opin
623 Virol, 2021. **49**: p. 36-40.
624 5. Owen, D.R., et al., *An oral SARS-CoV-2 M(pro) inhibitor clinical candidate for the treatment*
625 *of COVID-19.* Science, 2021. **374**(6575): p. 1586-1593.
626 6. Hammond, J., et al., *Oral Nirmatrelvir for High-Risk, Nonhospitalized Adults with Covid-*
627 *19.* N Engl J Med, 2022. **386**(15): p. 1397-1408.
628 7. Wong, C.K.H., et al., *Real-world effectiveness of early molnupiravir or nirmatrelvir-*
629 *ritonavir in hospitalised patients with COVID-19 without supplemental oxygen*
630 *requirement on admission during Hong Kong's omicron BA.2 wave: a retrospective cohort*
631 *study.* Lancet Infect Dis, 2022.
632 8. Reis, S., et al., *Nirmatrelvir combined with ritonavir for preventing and treating COVID-19.*
633 Cochrane Database Syst Rev, 2022. **9**(9): p. Cd015395.
634 9. Wen, W., et al., *Efficacy and safety of three new oral antiviral treatment (molnupiravir,*
635 *fluvoxamine and Paxlovid) for COVID-19 : a meta-analysis.* Annals of Medicine, 2022.
636 **54**(1): p. 516-523.
637 10. Vangeel, L., et al., *Remdesivir, Molnupiravir and Nirmatrelvir remain active against SARS-*
638 *CoV-2 Omicron and other variants of concern.* Antiviral Res, 2022: p. 105252.
639 11. Abdelnabi, R., et al., *The oral protease inhibitor (PF-07321332) protects Syrian hamsters*
640 *against infection with SARS-CoV-2 variants of concern.* Nat Commun, 2022. **13**(1): p. 719.
641 12. Unoh, Y., et al., *Discovery of S-217622, a Noncovalent Oral SARS-CoV-2 3CL Protease*
642 *Inhibitor Clinical Candidate for Treating COVID-19.* Journal of Medicinal Chemistry, 2022.
643 **65**(9): p. 6499-6512.
644 13. Mukae, H., et al., *A Randomized Phase 2/3 Study of Ensitrelvir, a Novel Oral SARS-CoV-2*
645 *3C-Like Protease Inhibitor, in Japanese Patients with Mild-to-Moderate COVID-19 or*
646 *Asymptomatic SARS-CoV-2 Infection: Results of the Phase 2a Part.* Antimicrob Agents
647 Chemother, 2022: p. e0069722.
648 14. Arnold, L.L., U, *Profile of PBI-0451 an Orally Administered 3CL Protease Inhibitor of SARS-*
649 *CoV-2 for COVID-19.* ICAR2022 meeting - Seattle, WA, 2022.
650 15. Boras, B., et al., *Preclinical characterization of an intravenous coronavirus 3CL protease*
651 *inhibitor for the potential treatment of COVID19.* Nat Commun, 2021. **12**(1): p. 6055.
652 16. Taylor, N. *Pfizer, in a rare COVID-19 setback, dumps Paxlovid's intravenous sibling in*
653 *further blow to ACTIV-3*. Available from: https://www.fiercebiotech.com/biotech/pfizer-
654 a-rare-covid-19-setback-dumps-paxlovid-s-intravenous-sibling-to-leave-activ-3-future.

17. Menéndez-Arias, L. and R. Delgado, *Update and latest advances in antiretroviral therapy.* Trends Pharmacol Sci, 2022. **43**(1): p. 16-29.
18. Ison, M.G., et al., *Influenza polymerase inhibitor resistance: Assessment of the current state of the art - A report of the isirv Antiviral group.* Antiviral Research, 2021. **194**: p. 105158.
19. Guo, C., et al., *Transmitted Drug Resistance in Antiretroviral Therapy-Naive Persons With Acute/Early/Primary HIV Infection: A Systematic Review and Meta-Analysis.* Front Pharmacol, 2021. **12**: p. 718763.
20. He, W., et al., *Distribution and evolution of H1N1 influenza A viruses with adamantanes-resistant mutations worldwide from 1918 to 2019.* J Med Virol, 2021. **93**(6): p. 3473-3483.
21. Focosi, D., et al., *Very low levels of remdesivir resistance in SARS-COV-2 genomes after 18 months of massive usage during the COVID19 pandemic: A GISAID exploratory analysis.* Antiviral Res, 2022. **198**: p. 105247.
22. Stevens, L.J., et al., *Mutations in the SARS-CoV-2 RNA dependent RNA polymerase confer resistance to remdesivir by distinct mechanisms.* Sci Transl Med, 2022: p. eabo0718.
23. Hogan, J.I., et al., *Remdesivir resistance in transplant recipients with persistent COVID-19.* Clinical Infectious Diseases, 2022: p. ciac769.
24. Hoffman, R.L., et al., *Discovery of Ketone-Based Covalent Inhibitors of Coronavirus 3CL Proteases for the Potential Therapeutic Treatment of COVID-19.* Journal of medicinal chemistry, 2020. **63**(21): p. 12725-12747.
25. Thi Nhu Thao, T., et al., *Rapid reconstruction of SARS-CoV-2 using a synthetic genomics platform.* Nature, 2020. **582**(7813): p. 561-565.
26. Moghadasi, S.A., et al., *Gain-of-Signal Assays for Probing Inhibition of SARS-CoV-2 M(pro)/3CL(pro) in Living Cells.* mBio, 2022: p. e0078422.
27. Gurard-Levin, Z.A., et al., *Evaluation of SARS-CoV-2 3C-like protease inhibitors using self-assembled monolayer desorption ionization mass spectrometry.* Antiviral research, 2020. **182**: p. 104924-104924.
28. Tomar, S., et al., *Ligand-induced Dimerization of Middle East Respiratory Syndrome (MERS) Coronavirus nsp5 Protease (3CLpro): IMPLICATIONS FOR nsp5 REGULATION AND THE DEVELOPMENT OF ANTIVIRALS.* J Biol Chem, 2015. **290**(32): p. 19403-22.
29. Zephyr, J., N. Kurt Yilmaz, and C.A. Schiffer, *Viral proteases: Structure, mechanism and inhibition.* Enzymes, 2021. **50**: p. 301-333.
30. Andreano, E., et al., *SARS-CoV-2 escape from a highly neutralizing COVID-19 convalescent plasma.* Proc Natl Acad Sci U S A, 2021. **118**(36).
31. Lee, J.T., et al., *Genetic Surveillance of SARS-CoV-2 M(pro) Reveals High Sequence and Structural Conservation Prior to the Introduction of Protease Inhibitor Paxlovid.* mBio, 2022. **13**(4): p. e0086922.
32. PfizerLaboratoriesDivPfizerInc, *FACT SHEET FOR HEALTHCARE PROVIDERS: EMERGENCY USE AUTHORIZATION FOR PAXLOVID™.* https://labeling.pfizer.com/ShowLabeling.aspx?id=16474, 2022.
33. Iketani, S., et al., *Multiple pathways for SARS-CoV-2 resistance to nirmatrelvir.* bioRxiv, 2022: p. 2022.08.07.499047.
34. Zhou, Y., et al., *Nirmatrelvir Resistant SARS-CoV-2 Variants with High Fitness in Vitro.* bioRxiv, 2022: p. 2022.06.06.494921.

699 35. Heilmann, E., et al., *SARS-CoV-2 3CL(pro) mutations selected in a VSV-based system confer*
700 *resistance to nirmatrelvir, ensitrelvir, and GC376.* Sci Transl Med, 2022: p. eabq7360.
701 36. Flynn, J.M., et al., *Comprehensive fitness landscape of SARS-CoV-2 Mpro reveals insights*
702 *into viral resistance mechanisms.* eLife, 2022. **11**: p. e77433.
703 37. Boudewijns, R., et al., *STAT2 signaling restricts viral dissemination but drives severe*
704 *pneumonia in SARS-CoV-2 infected hamsters.* Nat Commun, 2020. **11**(1): p. 5838.
705 38. Liu, C., et al., *Dual inhibition of SARS-CoV-2 and human rhinovirus with protease inhibitors*
706 *in clinical development.* Antiviral Res, 2021. **187**: p. 105020.
707 39. Jochmans, D., P. Leyssen, and J. Neyts, *A novel method for high-throughput screening to*
708 *quantify antiviral activity against viruses that induce limited CPE.* J Virol Methods, 2012.
709 **183**(2): p. 176-9.
710